Glass Europe Vol. 3 (2025) 125-146

https://doi.org/10.52825/glass-europe.v3i.2611

Submitted: 20 Feb. 2025 | Accepted: 08 Apr. 2025 | Published: 28 May 2025

Topological Modification and Elastic Softening of Sodium Borophosphate Glasses Through Substitution of Oxygen by Chlorine

Pengzhu Zhang[1], Courtney Calahoo[1], Jiangkun Cao[1], Alexis Duval[1], and Lothar Wondraczek[1,2,*]

[1]Otto Schott Institute of Materials Research, Friedrich Schiller University Jena, Fraunhoferstraße 6, 07743 Jena, Germany

[2]Center for Energy and Environmental Chemistry – CEEC, Friedrich Schiller University Jena, Philosophenweg 7, 07743 Jena, Germany

*Correspondence: Lothar Wondraczek, lothar.wondraczek@uni-jena.de

Abstract. Ionic glasses exhibit peculiar chemical formulations, atomic structures, and macroscopic properties. In particular, structure–property relationships cannot be explained using the classical network hypothesis; a standing challenge for understanding variations in ion mobility, vibrational dynamics and non-linear mixing effects. Here, we report on the substitution of oxygen by chlorine atoms in $[(Na_2O)_{0.4-x/2}(NaCl)_x](B_2O_3)_{0.48}(P_2O_5)_{0.12}$ glasses up to a substitution degree of around 10 %, effectively combining the enhanced electrical conductivity of halides and the chemical durability of oxide glasses. A mechanism of chlorine introduction, specific to borophosphate glasses, is proposed. The substitution of O^{2-} ions for Cl^- ions induces polymerization of the borophosphate network and conversion of BO_4 groups into BO_3 groups, thereby forming Na^+ and Cl^- enriched regions dispersed within a sodium-poor borophosphate network. Then, the associated increase in electrical conductivity and the dramatic changes in the elastic constants can be explained within the mixed random network model.

Keywords: Ionic Glass, Oxychloride, Structure, Electrical Conductivity, Elastic Properties

1. Introduction

Ionic glasses, where ionic cross-linking predominates over covalent bonding, exhibit increased configurational entropy, liquid fragility, Poisson's ratio, and ionic conductivity.[1], [2] Such properties stem from strong ionic interactions, which favor specific topologies and local structures with low structural dimensionality (*i.e.*, the absence of a percolating network according to conventional terms) and high local disorder: this glass family has gained considerable attention due to possible applications ranging from sensor components to energy and data storage, optics and biomedicine.

Adding halides (such as Li*X* and Na*X*; with *X* = F, Cl, Br, or I) to an oxide, sulfate or, e.g., sulfide glass has great consequences for the ionic conductivity and mechanical properties.[3-5] In NaCl-containing sulfate glasses, Na^+ and Cl^- ions are homogeneously distributed throughout the glass network, and are charge-compensated by the other glass constituting ions.[6] In $Na_2Si_3O_7$ and $CaSi_2O_5$ glasses doped with NaCl or $CaCl_2$, it was found that the local environment of Cl^- ions consists mostly of network modifiers (Na^+ and Ca^{2+}).[7]

Borophosphate glasses exhibit non-linear trends in structure and properties [8], [9], [10], [11], [12], strongly correlated with the type and concentration of network modifiers, and, more directly, with the BO_4 to BO_3 ratio. These glasses typically possess a low softening temperature, high electrical conductivity, and good chemical durability; they find use as glass solders, as host materials for high-power lasers,[13] for waste vitrification,[14] or as electrolytes in solid-state batteries. Hence, it is of interest to further investigate the tailoring of their properties through changes in their anionic composition.

Here, we elaborate on highly modified xNaCl-(40-x/2)Na_2O-48B_2O_3-12P_2O_5 glasses, where chlorine atoms substitute up to 10 % of the oxygen atoms. The emphasis is placed on understanding the compositional dependence of glass structure and the associated electrical and elastic properties.

2. Materials and Methods

2.1 Sample Preparation

A series of glasses with a nominal composition of $[(Na_2O)_{0.4-x/2}(NaCl)_x](B_2O_3)_{0.48}(P_2O_5)_{0.12}$, where x = 0.00, 0.05, 0.10, 0.15, 0.20, 0.25, and 0.30, was prepared by conventional melt quenching. The specific composition was chosen to maintain a fixed Na:B:P cation ratio, so as to vary only the anion composition, from nominal [Cl/(Cl+O)] = 0 to 12 %. Glass batches were prepared from analytical grade raw materials, NaCl, Na_2CO_3, H_3BO_3, and $NaPO_3$ (Carl Roth GmbH & Co. KG). Appropriate quantities of each reactant were thoroughly mixed to ensure proper homogeneity. Melting was conducted in an electric furnace. The mixed starting materials were melted in covered silica crucibles at temperatures ranging from 850 to 900 °C for one hour. The melts of the sample with $0 \leq x \leq 0.2$ were then cast into a graphite mold which was heated at around 30 °C below their T_g in another furnace, and the two most Cl-rich samples were cast on a copper plate and splat-quenched to prevent crystallization. All glass samples were annealed in air at around 30 °C below their T_g for one hour in the furnace. They were cooled down to room temperature by turning off the annealing furnace. The obtained glass samples were immediately transferred into a desiccator to prevent any reaction with ambient humidity. Before further characterization, the glass slabs were cut into square slices of approximately 10 mm × 10 mm × 2 mm, and polished to optical grade using oil–based dispersions of CeO_2 particles, with a final sample thickness of 2.0 mm.

2.2 Characterization

X-Ray diffraction (XRD) measurements were performed on powdered samples using a Rigaku Miniflex 600 diffractometer with CuK_α radiation (0.154 nm) in the 10 – 75° 2Θ range at a scanning rate of 5°/min.

A Jeol JSM-7001F scanning electron microscope (SEM) equipped with an energy-dispersive X-ray spectrometer (EDX) was used to conduct elemental analyses. The samples were coated with a carbon film to achieve a conductive surface prior to the measurements.

Differential scanning calorimetry (DSC) experiments were carried out using a NETZSCH STA 449F1 instrument, operating with a heating rate of 20 K/min. The glass transition temperature (T_g) was determined at the transition's onset points, while the crystallization temperature (T_c) was determined as the position of the associated exothermic peak.

The glass density was determined using the Archimedes method at 20 °C in ethanol (ρ = 0.78945 g/cm^3).

Raman spectra were collected in the 200 – 1300 cm^{-1} range with a Raman microscope (Renishaw inVia), equipped with a low-frequency notch filter, utilizing an excitation wavelength of 457 nm (Ar laser) in 90°scattering geometry. A confocal microscope with a 50x objective was used, and the Raman spectra were acquired for a duration of 90 s and averaged over 10 scans with a resolution of 2 cm^{-1}.

All Raman spectra were corrected for air scattering to further analyze the low-frequency range. For this, the reduced Raman intensity ($I^{red}(\omega)$) was calculated from the measured Raman intensity ($I_{meas}(\omega, T)$) as the product of reduced density of states ($g(\omega)/\omega^2$) and the coupling coefficient ($C(\omega)$), according to:

$$I^{red}(\omega) = \frac{I_{meas}(\omega,T)}{[n(\omega,T)+1]\omega} = C(\omega)\frac{g(\omega)}{\omega^2} \tag{1}$$

where $n(\omega,T) = [\exp\left(\frac{\hbar\omega}{k_B T}\right) - 1]^{-1}$ is the Bose–Einstein population factor for a given frequency ω and temperature T, k_B is the Boltzmann constant, and $\hbar$ is the reduced Planck constant. The Raman scattered light intensity depends both on the vibrational density of states and on the coupling efficacy between vibrations and photons. The empirical coupling coefficient is proportional to ω^{μ} ($0 \leq \mu \leq 2$), based on whether the excess in the vibrational density of states arises as hybrid modes, acoustic modes, or local optical modes. The following log–normal function was used to fit the asymmetry of the non-Debye low-frequency anomaly (we term this anomaly Raman boson peak (Raman BP) in the following); this was done in order to derive precisely and consistently the BP peak frequency ω_{BP}, following:

$$I(\omega) = A\exp\left\{-\ln 2\left[\frac{\ln\left(1+2\sigma\frac{\omega-\omega_{BP}}{w}\right)}{\sigma}\right]^2\right\} + I_0 \tag{2}$$

where A, σ, and w describe respectively the amplitude, asymmetry, and width of the function, while I_0 is an offset parameter.

A Fourier transform infrared (FTIR) spectrometer was employed to collect infrared transmittance and reflectance spectra on bulk glass samples, from 1600 to 4000 cm^{-1} and from 450 to 1600 cm^{-1}, respectively, at a 2 cm^{-1} resolution.

Magic-angle-spinning nuclear magnetic resonance (MAS-NMR) experiments were conducted with a Bruker Avance III 400 spectrometer, operating at a 9.4 T magnetic field, corresponding to a Larmor frequency of 162 MHz for ^{31}P. One-pulse 1D ^{31}P NMR experiments were performed with 60° pulses (2 μs) and a 350 s recycle time, employing 4 mm MAS probes in a Zirconia rotor and a sample rotation frequency of 12.5 kHz. All spectra were referenced to a 85 wt% H_3PO_4 solution.

Impedance measurements were performed using an Alpha-A High Performance Analyzer apparatus (Novocontrol). They were carried out at temperatures ranging from 50 to 250 °C in 25 °C increments, in the 10^{-1} to 10^7 Hz frequency range. The electrical conductivity (σ) was derived from Nyquist plots (where the imaginary part of impedance is plotted against the real part, *i.e.*, Z'' and Z' respectively), with the diameter of the semicircle taken as the direct current resistance (R_{DC}), according to:[15]

$$\sigma = \frac{1}{R_{DC}} \cdot \frac{l}{A} \tag{3}$$

where l and A are the thickness and the area of the sample, respectively. The temperature dependence of the electrical conductivity was described using an Arrhenian equation,

$$\sigma(T) = \frac{\sigma_0}{T}\exp\left(-\frac{E_A}{k_B T}\right) \tag{4}$$

where σ_0 is a pre-exponential factor, and E_A is the activation energy for the DC conductivity.

The elastic properties were determined by ultrasonic echography. The longitudinal (v_L) and transversal (v_T) sound velocities were measured using a piezoelectric transducer (Echometer 1077, Karl Deutsch GmbH &Co KG) with frequencies of 8 – 12 MHz. The shear modulus (G), bulk modulus (K), elastic modulus (E), and Poisson's ratio (v) were subsequently obtained according to:[16]

$$G = \rho v_T^2 \quad (5)$$

$$K = \rho\left(v_L^2 - \frac{4}{3} v_T^2\right) \quad (6)$$

$$E = \rho\left[\frac{3v_L^2 - 4v_T^2}{(v_L/v_T)^2 - 1}\right] \quad (7)$$

$$v = \frac{v_L^2 - 2v_T^2}{2(v_L^2 - v_T^2)} \quad (8)$$

3. Results and Discussion

3.1 Chlorine Solubility in Oxide Glasses

All synthesized samples were fully transparent, colorless and slightly hygroscopic. For further analysis, they were stored in silicate desiccant. The XRD patterns of the obtained $[(Na_2O)_{0.4-x/2}(NaCl)_x](B_2O_3)_{0.48}(P_2O_5)_{0.12}$ glasses are shown in Figure 1. For the Cl-free glass, the XRD profile exhibits various broad humps across the 10 – 75° range, confirming its amorphous nature. However, two distinct diffraction peaks are observed at 32 and 45° upon substitution of Na_2O for NaCl. These peaks are ascribed to crystalline NaCl, and are especially visible in the Cl-rich materials, *i.e.*, with $x \geq 0.25$. Hence, it appears that approximately 4 % of the total oxygen atoms can be nominally substituted by chlorine in these sodium borophosphate glasses before observing marked crystallization of sodium chloride.

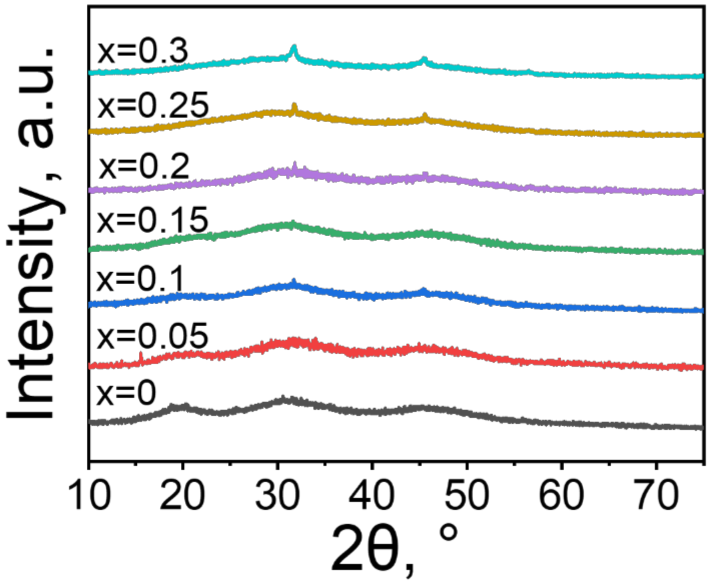

Figure 1. *XRD patterns of $[(Na_2O)_{0.4-x/2}(NaCl)_x](B_2O_3)_{0.48}(P_2O_5)_{0.12}$ glasses.*

***Table 1**. Nominal and experimentally determined atomic compositions (Na, P, Cl, and Si) of $[(Na_2O)_{0.4-x/2}(NaCl)_x](B_2O_3)_{0.48}(P_2O_5)_{0.12}$ glasses, derived from EDX measurements. The values in brackets indicate the statistical errors.*

Element	**Sample (*x*)**						
(at%)	0.00	0.05	0.10	0.15	0.20	0.25	0.30
Nom. Na	18	17.9	17.8	17.7	17.6	17.5	17.4
Exp. Na	23.3(0.1)	21.5(0.1)	23.3(0.1)	20.9(0.1)	21.5(0.1)	21.0(0.1)	20.8(0.1)
Nom. P	5.4	5.4	5.3	5.3	5.3	5.3	5.2
Exp. P	5.8(0.2)	5.6(0.1)	5.9(0.2)	5.4(0.2)	5(0.1)	5.4(0.2)	5.0(0.2)
Nom. Cl	0	1.1	2.2	3.3	4.4	5.5	6.5
Exp. Cl	0(0.1)	1.2(0.1)	2.4(0.2)	3.1(0.2)	4.1(0.1)	5.0(0.1)	5.8(0.2)
Exp. Si				0.27(0.1)			0.34(0.1)

The nominal and experimentally determined atomic compositions of the investigated glasses are summarized in Table **1** (error range in brackets). A good agreement was found for both P and Cl contents, which confirms the substitution of oxygen for chlorine. The Na content was found to be systematically larger than expected. This deviation is attributed to the transition from using $NaPO_3$ to NaCl as raw materials. Furthermore, a minor fraction of Si was observed in two of the samples, originating from silicate crucible dissolution. Overall, the experimentally determined atomic composition of the main elements Na : P : Cl was obtained as expected.

Figure **2**(a) and Figure **2**(b) depict the DSC curves and the glass transition temperatures (T_g) of the various glasses, respectively. The T_g decreases linearly with increasing Cl content, from 446 down to 374 °C. Although less evident, one can see that the crystallization temperature (T_c) also decreases as Cl substitutes for O. In the case of the most Cl-rich glass, the difference between T_c and T_g, indicative of the glass forming ability, is of the order of 30 K. Such a small value reflects a high tendency of the glass to crystallize upon quenching, which is in agreement with the diffraction peaks of NaCl previously observed. A well-defined endothermic peak is observed for the two most Cl-rich glasses, at approximately 800 °C. This process is ascribed to the melting of NaCl crystals. Therefore, it appears that the fraction of crystallized NaCl is more pronounced in only these two samples.

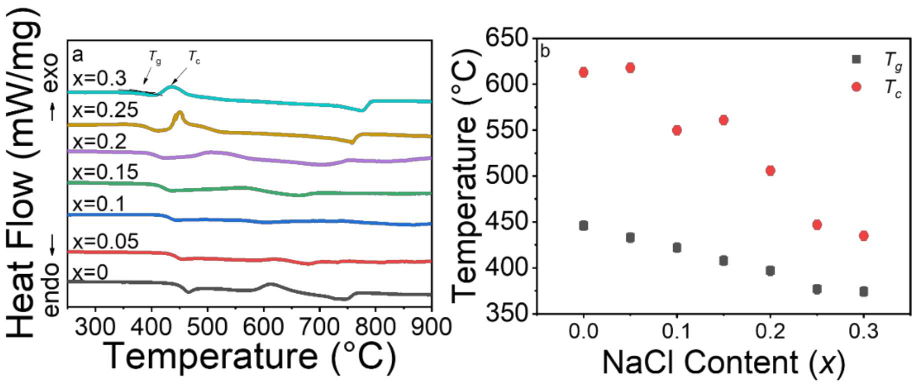

***Figure 2.** (a) DSC curves, and (b) glass transition temperature (T_g) and crystallization temperature (T_c) of $[(Na_2O)_{0.4-x/2}(NaCl)_x](B_2O_3)_{0.48}(P_2O_5)_{0.12}$ glasses, the error is within the symbol.*

3.2 A Structural Model for Oxychloride Glasses

Raman spectra of glasses facilitate the analysis of the network connectivity (P−O−B linkages), considering the contributions of PO_4 tetrahedra with different environments, *i.e.*, with varying PO_4 and BO_x next-nearest-neighbors. The $Q^n_{m,BOx}$ notation is introduced, where *n* represents the number of bonded PO_4 polyhedra, *m* the number of bonded BO_x polyhedra, and *x* the coordination state of boron, with $x = 3$ or 4. The Raman spectra of the glasses under study are shown in Figure **3**(a).

The spectrum exhibits its stronger bands in the region from 600 to 1160 cm^{-1} and a number of weaker bands at lower frequencies, in the range of 250 – 600 cm^{-1}, with another band at 1228 cm^{-1}. In the lower frequency range, bands at 325, 485, and 554 cm^{-1} are observed, the band at 325 cm^{-1} is assigned to the P-O-P bending vibrations of phosphate lattice, while the other two bands could be related to the bending vibrations of O-P-O in borophosphate and/or phosphate chains according to a previous study.[17] The band at 1228 cm^{-1} (with increasing intensity as chlorine substitutes for oxygen) could be due to $Q^0_{3,BOx}$ when $0.1 \leq x$. [18]

In the s area from 600 to 1160 cm^{-1} multiple overlapping Raman bands are attributed to borate and interconnected borophosphate networks. To better identify and quantify the underlying structural changes, the Raman spectra in this range are deconvoluted using 11 Gaussian contributions, each corresponding to specific vibrational modes: (1) P-O-B stretching vibrations in Q^2 units (630 cm^{-1}), [18] (2) bending modes of metaborate chains $BO_2{\cdot}NBO^-$ (673 cm^{-1}), (3) vibrational modes of borate rings consisting of one trigonal BO_3 group and two tetragonal BO_4 groups (715 cm^{-1}), (4) vibrational modes of borate rings consisting of two BO_3 groups and one BO_4 group (766 cm^{-1}), (5) vibrational modes of three BO_3 groups in boroxol rings (800 cm^{-1}), [9,], [19], [20], [21], [22](6) modes indicative of the presence of pentaborate (895 cm^{-1}),[21] (7) stretching mode of the BO_4^- tetrahedra (947 cm^{-1}),[20] (8) vibrational mode of $Q^0_{1,BOx}$ (980 cm^{-1}),[18] (9) symmetric stretching vibrations of phosphate terminal tetrahedra connected with tetrahedral or trigonal boron units in $Q^1_{1,BOx}$ (1015 cm^{-1}), (10) symmetric stretching vibrations P-O^- of phosphate terminal tetrahedra in $Q^1_{1,BOx}$ (1070 cm^{-1}),[23] (11) symmetric stretching mode of $Q^0_{2,BOx}$ (1108 cm^{-1})[18]. Note that the positions of each Raman band slightly shift with increasing fraction of Cl^- ions, while some are no longer observed in Cl-poor glasses. The results are presented in Figure **3**(b). The relative intensity of the deconvoluted peaks in this region with standard error is shown in Figure **3**(c). According to Yano *et al.*'s study the Raman band intensities regarding to borates were found to be correlated quite well with the results of ^{11}B NMR spectroscopy,[24] therefore, the relative fractions of BO_3 and BO_4 groups are then derived from the areas of the vibrational modes of the present glass samples (Figure **3**(d)). As chlorine substitutes for oxygen, numerous changes in relative intensity and position of the vibrational modes occur, indicative of reorganizations of the glass network. Specifically, the decrease of the relative intensity of peak (8) and the increase of peak (11) suggest that the unit $Q^0_{1,BOx}$ is converted to $Q^0_{2,BOx}$. In addition, the increase of peak (9) indicates that the phosphate tetrahedra with P-O bonds involving NBOs become more connected to borate units. A clear trend emerges, wherein the fraction of BO_4 groups (*i.e.*, the $[BO_4/(BO_4+BO_3)]$ ratio) experiences a linear drop from 59 % down to 52 % as *x* increases from 0.00 to 0.2, followed by nearly no changes with further addition of chlorine. This indicates that the structural rearrangement of the glass network follows a two-step process. From $x = 0.00$ to $x = 0.2$, Cl^- ions promote the conversion of BO_4 groups into BO_3 groups, while another mechanism prevails starting from $x = 0.25$.

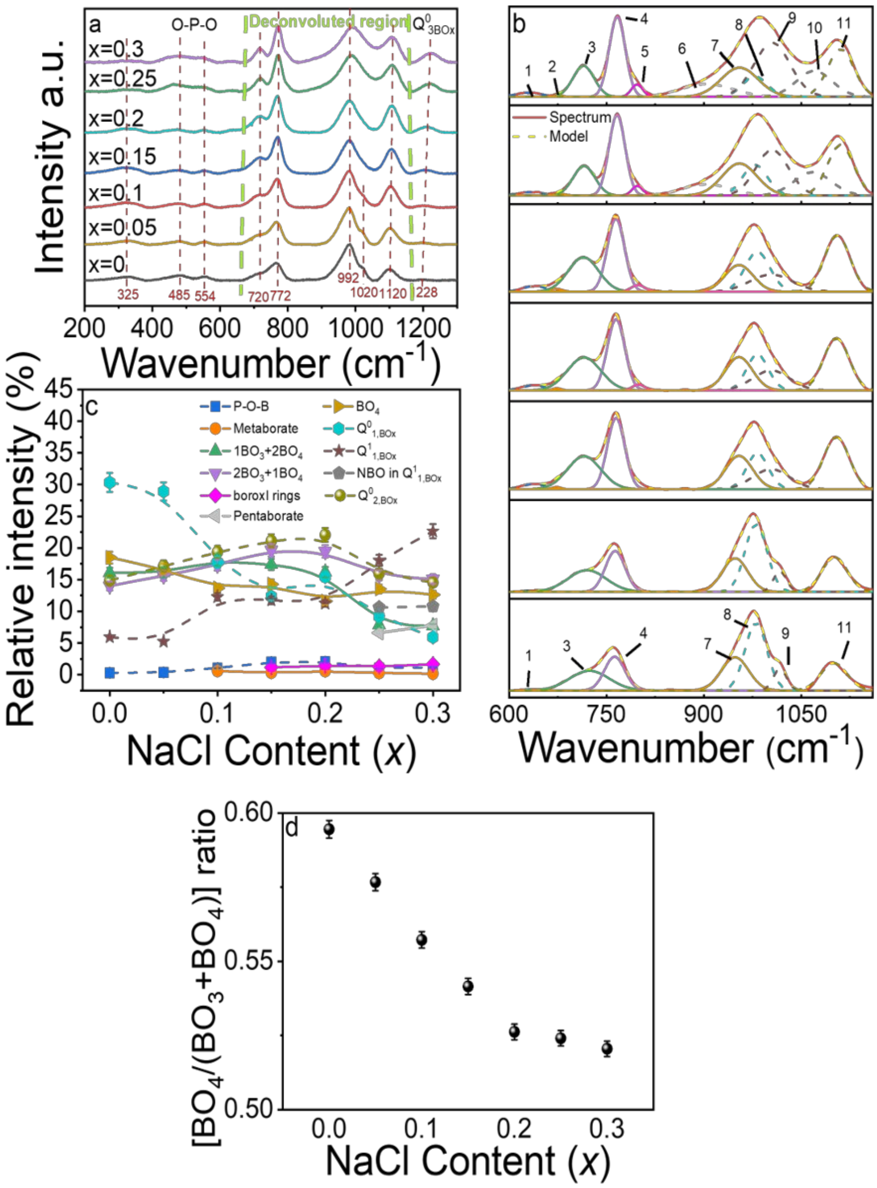

Figure 3. *Raman spectra in the 200 – 1300 cm^{-1} range, (b) deconvolution of the vibrational modes in the 600 – 1160 cm^{-1} range, deconvoluted peaks with different number are discussed above, and (c) relative intensity of the deconvoluted peaks calculated from the integral of the peak area, with solid lines relating to the borate units and dashed lines relating to the phosphate units, and (d) compositional dependence of the* $[BO_4/(BO_4+BO_3)]$ *ratio of* $[(Na_2O)_{0.4-x/2}(NaCl)_x](B_2O_3)_{0.48}(P_2O_5)_{0.12}$ *glasses.*

Figure 4(a) shows the reduced low frequency 0 – 200 cm^{-1} Raman spectra of the glass samples. The derived compositional dependence of the BP's frequency (ω_{BP}) is presented in Figure 4(b). One can clearly see a nearly linear decrease, from 59 down to 52 cm^{-1}, as chlorine gradually substitutes for oxygen. The boson peak is commonly associated with a degree of disorder in the intermediate to long-range order structural length scale.[25], [26], [27] In a pragmatic consideration, it serves as a signature of structural inhomogeneity on the scale of a few nanometers, as proposed in the non-continuous vitreous structural model developed by Duval *et al.*[28] The model assumes the existence of cohesive domains, within which the atoms are more strongly linked with respect to atoms located outside of these domains. Consequently, the average length scale of dynamic heterogeneity is inversely proportional to the BP frequency. The shift in BP frequency observed in this study thus reflects an increased heterogeneity of the glass network, *e.g.*, through non-random distributions of ions, or through bonding preferences.[29]

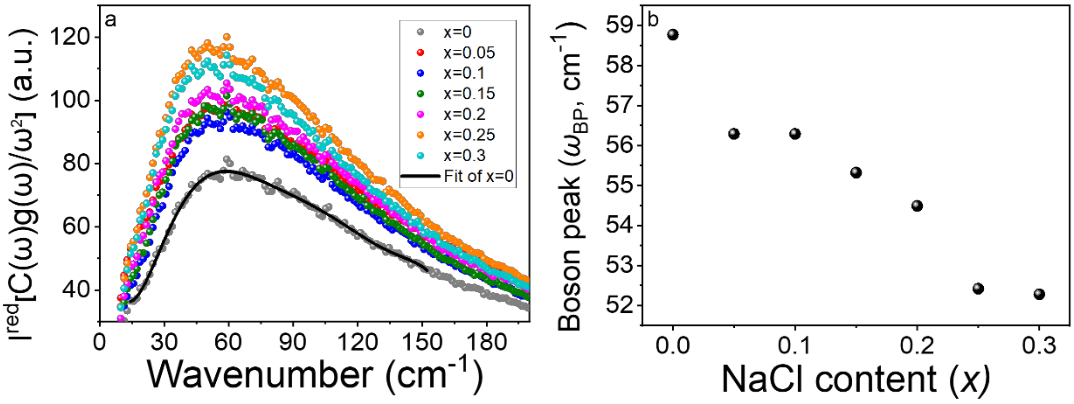

***Figure 4**. (a) Reduced low–frequency Raman spectra in the 0 – 200 cm^{-1} range, and (b) compositional changes in Boson peak's frequency (ω_{BP}) of $[(Na_2O)_{0.4-x/2}(NaCl)_x](B_2O_3)_{0.48}(P_2O_5)_{0.12}$ glasses (error bar is within the symbol).*

Complementarily, the vibrational modes present in the FTIR-absorbance spectra of the various glasses (see Figure **5**(a)) are identified following previous works.[30], [31], [32] As observed using Raman spectroscopy, numerous vibrational modes characteristic of phosphate and borate networks are reconfirmed: vibrations of bridging P-O-P linkages (820 cm^{-1}), deformation of P-O bonds (560 cm^{-1}), bending of bridging B-O-B linkages (695 cm^{-1}), stretching of BO_4 groups (948 cm^{-1}), and stretching of BO_3 groups (1475 cm^{-1}). The vibrational modes of BO_3 groups, and those of non-bridging O-P-O linkages, are superposed at 1370 cm^{-1}.

Considerable shifts in position and relative intensity of several vibrational modes, specifically involving B-O-B and P-O-P linkages, as well as disappearance of terminal P=O bonds (1090 cm^{-1}), strongly suggest the incorporation of phosphate chains into the borate network following chlorine addition. Moreover, the peak at 1210 cm^{-1} indicates an increase of BO_4 units. Therefore, the glass network mainly consists of chains and rings of BO_3 and BO_4 groups interconnected through B-O-B linkages, alongside PO_4 tetrahedra connected to other PO_4 tetrahedra and to BO_x groups through P-O-P and P-O-B linkages. Sodium ions act as network modifiers, and are neighboring both PO_4 and BO_x structural units.

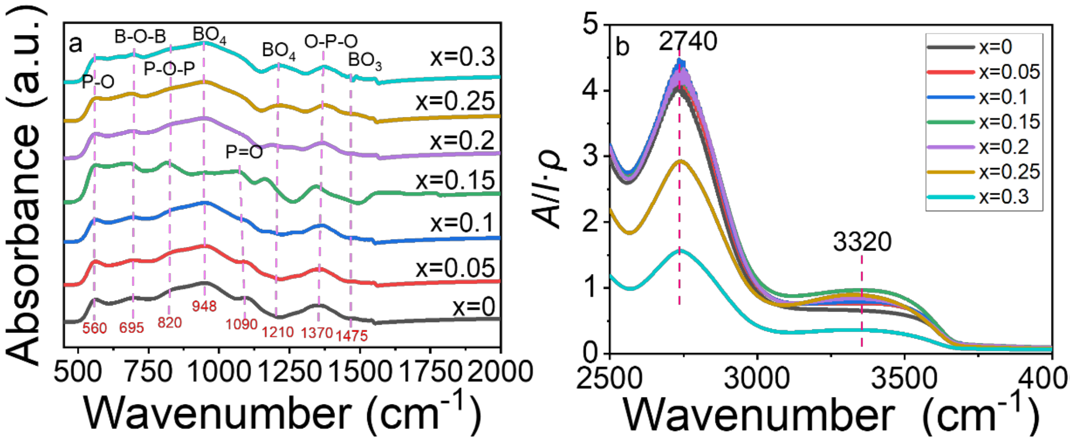

***Figure 5.** FTIR-absorbance spectra of $[(Na_2O)_{0.4-x/2}(NaCl)_x](B_2O_3)_{0.48}(P_2O_5)_{0.12}$ glasses (a) in the 450 – 2000 cm^{-1} range, and (b) calculated $A/l\cdot\rho$ vs. IR frequency from raw FTIR-transmittance spectra in the 2500 – 4000 cm^{-1} range.*

FTIR-absorbance spectra in the near infrared provide insights into the water content of glasses. Typically, three characteristic bands associated with -OH bonds are observed at 2350 cm^{-1}, and in the 3300 – 3640 cm^{-1} and 2600 – 3000 cm^{-1} ranges.[33], [34], [35], [36] Hence, the determination of the total water content requires a summation of all three bands, using the area of each absorption band (*A*) following the Beer-Lambert law:[37], [38], [39]

$$c = \frac{18.02A}{l\rho\varepsilon} \tag{9}$$

$$c = \frac{A}{l\varepsilon} \tag{10}$$

where *c* is the water concentration in wt% (equation (9)) or in mol·L^{-1} (equation (10)), ε is the molar extinction coefficient for water, and *l* and ρ denote the sample thickness and mass density, respectively. In previous literature, ε slightly varies across different glass chemical systems, and typically ranges from 88 to 115 L·mol^{-1}·cm^{-1}.[40] A value of 98 L·mol^{-1}·cm^{-1} was used for this study.

Table 2*. Calculated water content, obtained individually and in total for each $[(Na_2O)_{0.4-x/2}(NaCl)_x](B_2O_3)_{0.48}(P_2O_5)_{0.12}$ glass, from FTIR-absorbance spectra at 3320 cm^{-1} and 2740 cm^{-1}.*

Sample (*x*)		**$c_{\mathrm{H_2O}}$ at 3320 cm^{-1}**		**$c_{\mathrm{H_2O}}$ at 2740 cm^{-1}**		**$c_{\mathrm{H_2O}}$ in total**	
		wt%	**mol·L^{-1}**	**wt%**	**mol·L^{-1}**	**wt%**	**mol·L^{-1}**
0.00		0.025	0.004	0.155	0.021	0.180	0.025
0.05		0.029	0.004	0.160	0.021	0.189	0.025
0.10		0.030	0.004	0.163	0.022	0.193	0.026
0.15		0.037	0.005	0.162	0.021	0.199	0.026
0.20		0.032	0.004	0.161	0.021	0.193	0.025
0.25		0.051	0.007	0.167	0.021	0.218	0.028
0.30		0.040	0.005	0.172	0.022	0.212	0.027

The calculated *A*/*l*·*ρ* vs. IR frequency from raw FTIR-transmittance spectra of the investigated oxychloride glasses in the 2500 – 4000 cm^{-1} range are displayed in Figure 5(b). Only two distinct absorption bands peaking at 2740 and 3320 cm^{-1} are identified, due to the small intensity and overlap of the third band. As summarized in Table 2, the calculated water contents are small (< 0.3 wt%, or < 0.03 mol·L^{-1}), and are nearly independent of the chlorine content. The resultant random error in the transmittance is no more than ± 0.03%. The effect of water on the changes in glasses macroscopic properties was therefore disregarded in the following.

1D ^{31}P MAS-NMR spectra of the glass series are shown in Figure 6(a). The Cl-free glass exhibits two main peaks at 4.5 and –4.5 ppm, characteristic of P^1 and P^2 units, where the superscript refers to the number of bridging oxygens, whether in P-O-P or P-O-B linkages to PO_4, BO_3 or BO_4 units. Further substitution of oxygen by chlorine induces a change in position of said peaks towards lower chemical shifts, as well as a commensurate broadening, indicative of superimposed peaks, *i.e.,* additional structural units.

To reach a deeper understanding of the complex structure of oxychloride glasses, the obtained 1D ^{31}P MAS-NMR spectra were deconvoluted considering the contributions of PO_4 tetrahedra in different environments, *i.e.*, with varying PO_4 and BO_x next-nearest-neighbors. The fits were made on the basis of 1D and 2D ^{31}P solid-state NMR data from previous works, performed on similar borophosphate and phosphate glasses,[41], [42], [43]using the DMFIT software.[44] They are presented in Figure 6(b). Based on the chemical shifts, which are directly correlated with the nature and number of neighboring structural units, and full widths at half maximum of each structural unit, various $Q^n_{m,BOx}$ environments are identified, from largest to smallest in ppm: $Q^0_{0,BOx}$, $Q^1_{0,BOx}$, $Q^0_{1,BOx}$, $Q^0_{2,BOx}$, $Q^0_{3,Box}$, and, $Q^1_{1,Box}$. The $Q^1_{0,BOx}$ and $Q^0_{1,BOx}$ peaks are close together, we assign them both based on Raguenet *et al.*'s work[41], however, Tricot *et al.* assigned these two peaks in the opposite order.[45] However, due to the difficulty in decomposing the broad and complicated 1D ^{31}P NMR spectra from borophosphate glasses, both assignments could be possible in our work. This ambiguity does not affect our conclusions. [46] After the Monte Carlo uncertainty calculations the absolute error of the fitting parameters is less than 0.1 ppm.

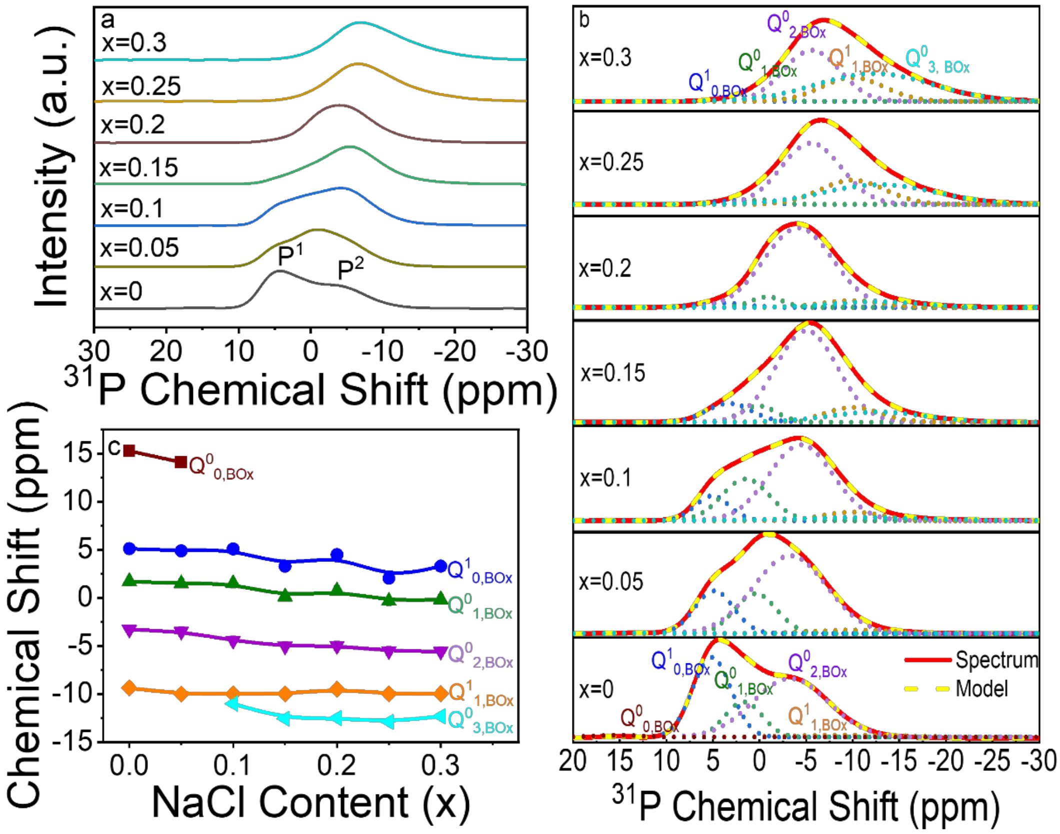

Figure 6. *(a) 1D ^{31}P MAS-NMR spectra of $[(Na_2O)_{0.4-x/2}(NaCl)_x](B_2O_3)_{0.48}(P_2O_5)_{0.12}$ glasses, and (b) deconvolution of the ^{31}P 1D MAS-NMR spectra into various $Q^n_{m,BOx}$ structural units. (c) Compositional dependence in chemical shift of the various $Q^n_{m,BOx}$ structural units.*

Although the chemical shifts of each structural unit are independent of the Cl content (see Figure 6(c)), great changes are observed with respect to their proportions (shown in Figure 7(a)). While the glass network is initially predominantly constituted of $Q^0_{2,BOx}$ (50 %) along with $Q^1_{0,BOx}$ (35 %) and $Q^0_{1,BOx}$ (15 %) structural units, $Q^1_{0,BOx}$ and $Q^0_{1,BOx}$ are gradually substituted for $Q^0_{2,BOx}$, $Q^1_{1,BOx}$ and $Q^0_{3,BOx}$ as x increases from 0.00 to 0.20. Starting from $x = 0.25$, $Q^0_{2,BOx}$ structural units are also replaced by $Q^0_{3,BOx}$.

Hence, in a first step ($x \leq 0.20$), PO_4 tetrahedra form more P-O-B linkages with BO_x polyhedra (m increases). This is accompanied by a decrease in NBO per PO_4 tetrahedra (represented in Figure 7(b)), *i.e.*, by a polymerization between phosphate and borate networks. In a second step ($x \geq 0.25$), $Q^0_{2,BOx}$ structural units convert to $Q^0_{3,BOx}$, *i.e.*, P-O-P linkages form at the expense of P-O-B linkages. This behavior occurs at similar concentrations of Cl^- ions as (i) the plateauing of the $[BO_4/(BO_4+BO_3)]$ ratio derived from Raman spectra, and (ii) the crystallization of NaCl during quenching. We infer that the conversion of BO_4 groups into BO_3

groups is strongly intertwined with the formation of P-O-B linkages, but also with chlorine solubility.

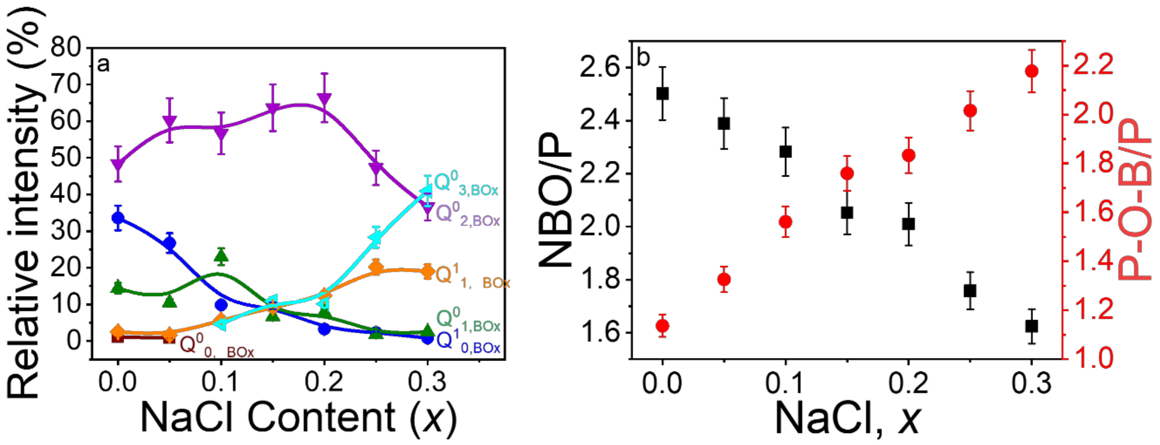

Figure 7. *(a) Relative intensity of the various* $Q^n_{m,BOx}$ *structural units in* $[(Na_2O)_{0.4-x/2}(NaCl)_x](B_2O_3)_{0.48}(P_2O_5)_{0.12}$ *glasses derived from the corresponding 1D* ^{31}P *MAS-NMR spectra. (b) Number of NBO (square symbols) and P-O-B linkages (round symbols) per P tetrahedra derived from the relative intensity of the various* $Q^n_{m,BOx}$ *structural units.*

From the various and highly consistent insights provided by Raman spectra, FTIR-absorbance spectra, and 1D ^{31}P MAS-NMR spectra of the obtained glasses, we now infer the local environment of chloride ions and, ultimately, suggest a structural model for sodium borophosphate oxychloride glasses. Indeed, the introduction of Cl^- ions induces changes both in the connectivity (formation of P-O-B linkages) and in the polymerization degree (decrease of the NBO/P ratio) of the glass network. Yet, the oxygen to chlorine ratio is the sole variable in the investigated glass compositions. Hence, we propose that sodium ions, initially participating in P-O··Na and B-O··Na linkages, preferentially situate in the first coordination sphere of Cl^- ions, thereby forming Na^+ and Cl^- enriched regions embedded inside the borophosphate network. This is supported by the study of Sandland *et al.*,[7] where the local environment of Cl^- ions in silicate and aluminosilicate glasses mostly consisted of network modifiers, and by the increased structural inhomogeneity which is suggested from the shift in the boson peak frequency.

The Cl-free glass structure is depicted in Figure **8**(a). The structural changes resulting from the substitution of an oxygen atom by two chlorine atoms can be summarized in the following equations:

$$2PO{\cdot\cdot}Na^+ + 2Cl^- \rightarrow P\text{-}O\text{-}P + 2NaCl + O^{2-} \tag{11}$$

$$2BO_4{\cdot\cdot}Na^+ + 2Cl^- \rightarrow 2BO_3 + 2NaCl + O^{2-} \tag{12}$$

$$PO{\cdot\cdot}Na^+ + BO_4{\cdot\cdot}Na^+ + 2Cl^- \rightarrow P\text{-}O\text{-}BO_2 + 2NaCl + O^{2-} \tag{13}$$

Schematically, Na^+ ions (highlighted in red in Figure 8(b)) migrate out of the borophosphate network and form Na^+ and Cl^- enriched regions (highlighted in green in Figure 8(c)), leaving behind a glass network with a higher crosslinking density through the formation of P-O-B and P-O-P linkages, yet with decreased dimensionality through the conversion of BO_4 groups to BO_3 groups. Hence, the presence of BO_4 groups is crucial to enable large solubilities of Cl^- ions in oxide glasses. This decrease in network dimensionality is reflected through the gradual decrease in T_g upon chlorine addition (see Figure 2(b)), in agreement with previous observations in some other glass systems, although it is not a universal phenomenon.[47], [48], [49] Nevertheless, when the concentration and size of these enriched regions reach a critical volume fraction ($x \geq 0.25$), crystallization of NaCl occurs during quenching (see Figure 1).

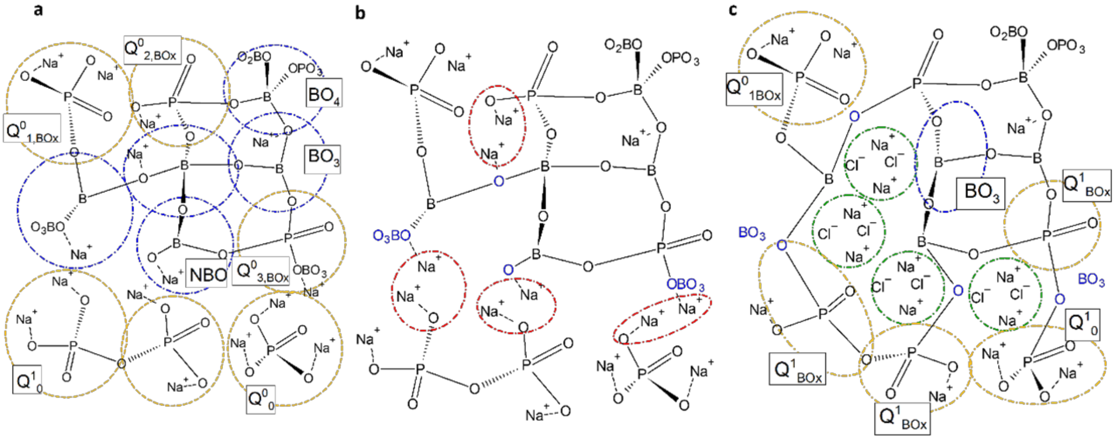

Figure 8. *(a) Suggested structural model of sodium borophosphate glasses composed of BO_3 and BO_4 structural units (blue), as well as $Q^0_{0,BOx}$, $Q^1_{0,BOx}$, $Q^0_{1,BOx}$ $Q^0_{2,BOx}$, and $Q^0_{3,Box}$ PO_4 structural units (yellow). (b) Identification of Na^+ ions (red) prone to form Na^+ and Cl^- enriched regions. (c) Structural model of sodium borophosphate oxychloride glasses, with Na^+ and Cl^- enriched regions (green), and newly formed BO_x (blue) and $Q^n_{m,BOx}$ (yellow) structural units.*

3.3 Electrical and Elastic Properties

The Nyquist plot of Cl-free glass, consisting of a typical semicircle, is shown in Figure 9(a). The red points, associated with the double layer effect, are not considered. The temperature dependence of the electrical conductivity with increasing Cl content is shown in Figure 9(b). No deviations from an Arrhenian behavior are observed. The electrical conductivity is on the order of 10^{-8} S/cm at 50 °C for the Cl-free glass; it increases roughly linearly by one order of magnitude as oxygen atoms are substituted by chlorine atoms, albeit showing a sudden drop in the most Cl-rich glass (see Figure 9(c)). Interestingly, the activation energy for DC conductivity (E_A) shows an abrupt increase of 0.2 eV as x increases from 0.00 to 0.05, and no further changes upon further introduction of chlorine (shown in Figure 9(d)). This is indicative of similar ion mobility mechanisms across the various glass compositions, presumably closely connected to the structural effect of Cl^- ions on Na^+ mobility.

First, we infer that the compositional dependence of the electrical conductivity is unrelated to the water content. While it is known that protonic conduction can play a significant role in phosphate glasses,[36], [37], [38] this effect is minor: in $MO\text{-}P_2O_5$ (M = Mg, Ca, or Ba) glasses, an increase in water concentration from 0.03 mol·L^{-1} to 0.10 mol·L^{-1} resulted in an increase of electrical conductivity by only 10^{-10} S/cm (measured at 144 °C).[33], [37] In the present study, the largest change observed in water concentration is an order of magnitude smaller, while the changes in electrical conductivity are on the order of 10^{-8} S/cm. They are thus ascribed to mechanisms of a different nature.

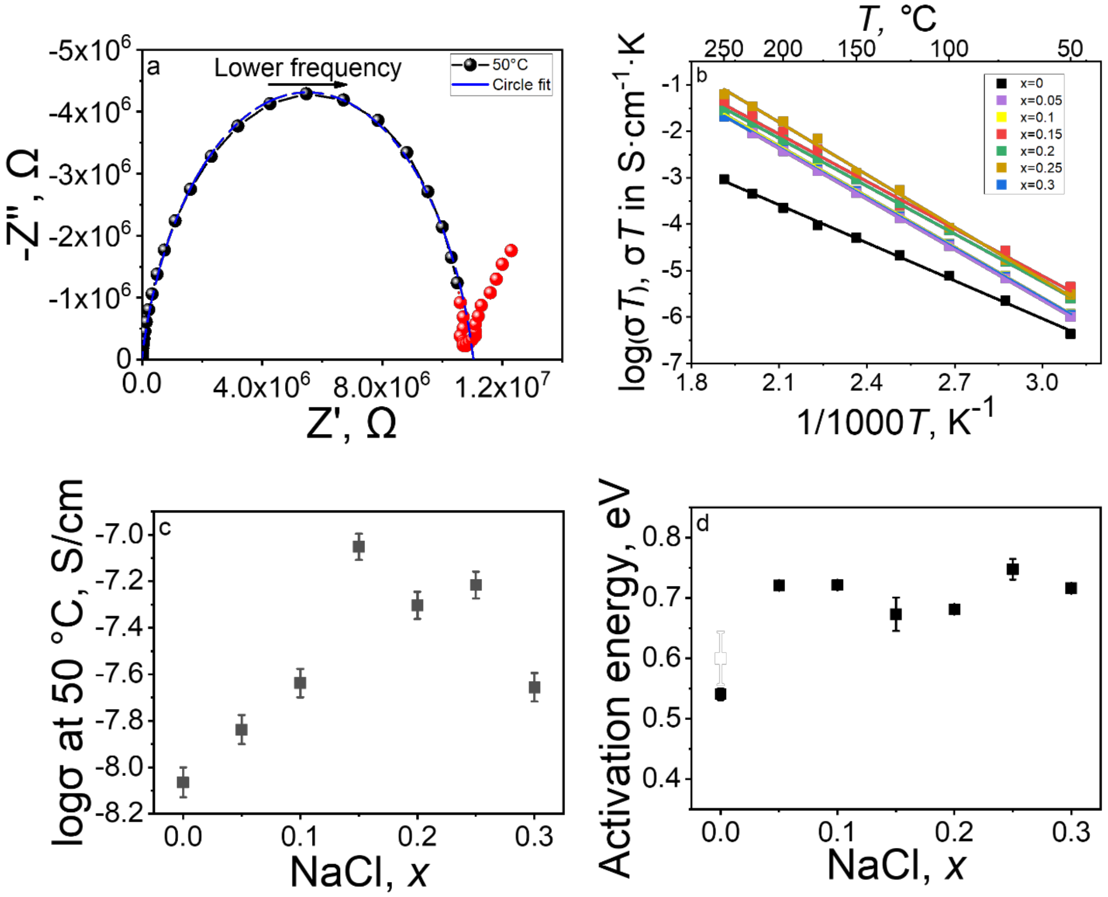

Figure 9. *(a) Nyquist plot of the Cl-free glass* $(Na_2O)_{0.4}(B_2O_3)_{0.48}(P_2O_5)_{0.12}$ *measured at 50 °C. Red points, ascribed to the double layer effect, are not considered. (b) Temperature dependence of the electrical conductivity of* $[(Na_2O)_{0.4-x/2}(NaCl)_x](B_2O_3)_{0.48}(P_2O_5)_{0.12}$ *glasses. (c) Compositional dependence of the electrical conductivity of* $[(Na_2O)_{0.4-x/2}(NaCl)_x](B_2O_3)_{0.48}(P_2O_5)_{0.12}$ *glasses measured at 50 °C. (d) Compositional dependence of the activation energy for DC conductivity of* $[(Na_2O)_{0.4-x/2}(NaCl)_x](B_2O_3)_{0.48}(P_2O_5)_{0.12}$ *glasses.*

Compositional dependence of the electrical conductivity showing a local maximum was previously observed in numerous glass systems, *e.g.*, when B_2O_3 substitutes for P_2O_5 in sodium borophosphate glasses,[50] or in ternary Li_2O-P_2O_5-LiX glasses (X = I, Br, or Cl) with increasing LiX content.[51] Multiple arguments were put forward to elucidate this phenomenon. Among these, the non-linear changes in (1-x)K_2O-xLi_2O-2SiO_2 glasses electrical conductivity were explained in the light of Greaves's modified random network (MRN) model, considering that "foreign" cations become "stuck" within the conduction channels and thus effectively block the motion of cations belonging to the initial host glass.[52]

In the present study, the increase in electrical conductivity following the introduction of Cl^- ions is greatly interlinked with the Na^+ and Cl^- enriched regions, and can be explained based on the MRN model. For small chlorine concentrations ($x \leq 0.20$), Na^+ ions preferentially localize with Cl^- ions in the channels outside the borophosphate network. Sodium ions, no longer closely bonded to the glass network through P-O-Na and B-O-Na linkages, exhibit increased mobility and become efficient charge carriers.[53] However, at large chlorine concentrations ($x \geq 0.25$), the considerable increase in polymerization degree of the glass network (NBO/P decreases from 2.5 to 1.8 as x increases from 0.00 to 0.30) both hampers the mobility of Na^+ ions, and promotes the segmentation of percolation channels, ultimately forming isolated Na^+ and Cl^- enriched regions and effectively confining charge carriers.[54] The intricate interplay between these two mechanisms thus sheds light on the dependence of the electrical conductivity on increasing substitution of O^{2-} ions by Cl^- ions in sodium borophosphate oxychloride glasses. The structural models of Cl-poor and Cl-rich sodium borophosphate glasses are represented schematically using the MRN model in Figure 10(a) and Figure 10(b), respectively.

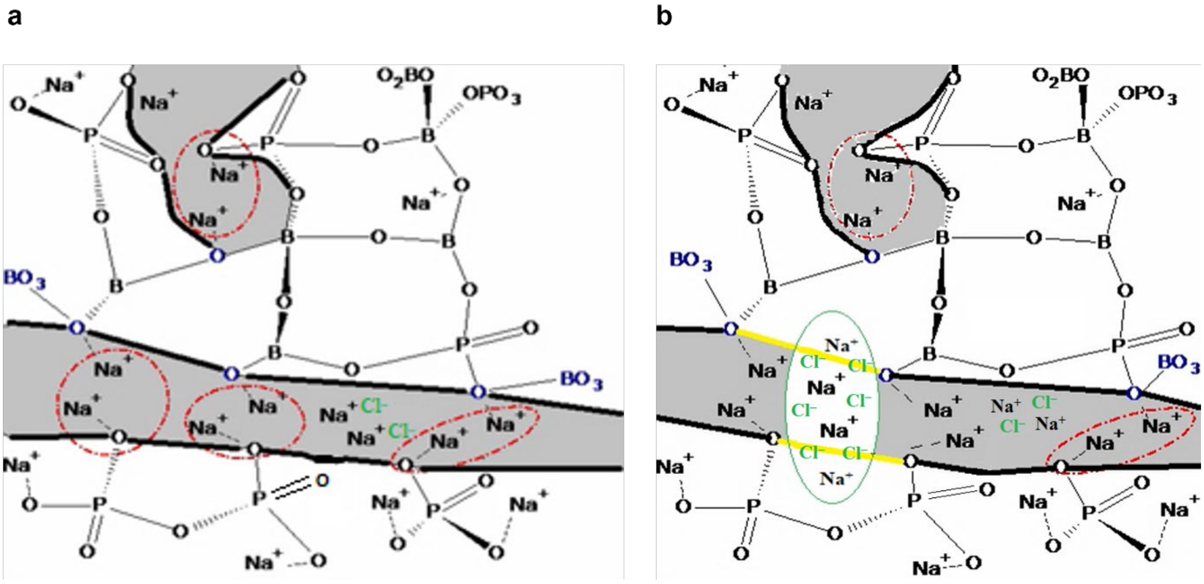

Figure 10. *MRN model for* $[(Na_2O)_{0.4-x/2}(NaCl)_x](B_2O_3)_{0.48}(P_2O_5)_{0.12}$ *glasses, after Greaves.[55] Unshaded areas correspond to network former regions, while shaded areas highlight the percolation channels for cation diffusion, (a) with small concentrations of* Cl^- *ions (*$x \leq 0.20$*), and (b) with large concentrations of* Cl^- *ions (*$x \geq 0.25$*). Covalent bonds are represented with solid lines, and ionic bonds with dotted lines.*

The molar volume (V_m) of the various glass samples is calculated from the corresponding glass composition and density, according to:

$$V_m = \frac{\Sigma f_i M_i}{\rho} \tag{14}$$

where f_i and M_i are the atomic fraction and the molar mass of the i^{th} constituting element, respectively. From there, the packing density (C_g) is calculated following:

$$C_g = \frac{N_A \Sigma \frac{4}{3} \pi f_i {r_i}^3}{V_m} \tag{15}$$

where r_i is the ionic radius of the i^{th} constituting element, and N_A is the Avogadro number. It is representative of the efficiency of element packing in a given matrix.

The density and the molar volume of the investigated glasses are shown in Figure 11(a), while the corresponding packing density is depicted in Figure 11(b). As x increases from 0.00 to 0.30, *i.e.*, as O^{2-} ions ($r_{O^{2-}}$ = 1.35 Å) are substituted by larger Cl^- ions (r_{Cl^-} = 1.81 Å)[56], the density of the glasses decreases from 2.46 to 2.27 g/cm^3, and the molar volume oppositely increases from 37.5 to 38.5 cm^3/mol. Nevertheless, these compositional changes translate but to very slight changes in glass packing density. Indeed, it can be considered fairly independent from the chlorine content, standing at a nearly constant value of 56 %.

The shear modulus (G), bulk modulus (K), and elastic modulus (E) of the glasses under study are presented in Figure 11(c). The Poisson's ratio (v) is plotted separately in Figure 11(d). Indeed, while G, K, and E all dramatically decrease by approximately 60 % as x increases from 0.00 to 0.30, v shows a surprising opposite behavior and increases from 0.213 to 0.248. One can also note the abrupt decrease in G, K, and E when x exceeds 0.20, stemming from the large fraction of crystallized NaCl.

Following the model of Makishima and Mackenzie, both an increase in volume density of energy (G_i) of the glass constituents and in glass packing density are expected to lead to an increase in the elastic modulus[57]:

$$E = 2C_g\Sigma g_i G_i \tag{16}$$

where g_i is the molar fraction of each glass constituent, and G_i is calculated from the molar dissociation energy of the constituent oxides and chlorides. However, one can clearly see that the changes in packing density are too small (< 0.5 %) to account for the sudden drop in elastic modulus, from 77.1 down to 32.5 GPa, as chlorine atoms substitute for oxygen atoms. In addition, (i) sodium forms stronger bonds with chlorine than oxygen (412 kJ/mol for Na-Cl bonds, and 270 kJ/mol for Na-O bonds), and (ii) the molar dissociation energy of NaCl is larger than that of Na_2O (320 and 294 kJ/mol, respectively[58], [59]). Hence, one would intuitively expect an increase in elastic modulus based solely from these simple approaches. Furthermore, while it is well known that increasing packing density leads to a noticeable increase in Poisson's ratio, it is evident that the striking increase in Poisson's ratio observed here finds its origins elsewhere.

Based on the previously presented MRN model of sodium borophosphate oxychloride glasses, their glass structure can be seen as a superposition of (i) a network modifier-poor borophosphate glass, with (ii) Na^+ and Cl^- enriched regions of varying sizes. The former usually show small elastic moduli (< 40 GPa) due to lower polymerization between phosphate and borate, while the second can be found comparable to crystalline NaCl, for which *E* is close to 40 GPa[60]. Therefore, the elastic moduli gradually decrease as Na^+ ions migrate away from the borophosphate network, and the volume fraction of these enriched regions increases. This is further accentuated as NaCl crystallizes during quenching.

The introduction of 1-fold Cl^- ions at the expense of 2-fold O^{2-} ions increases the cross-linking density of the glass network, but also induces the conversion of BO_4 groups into BO_3 groups. This mechanism effectively decreases the dimensionality of the glass network, as tridimensional structural units are converted to bidimensional structural units, which further translates into a smaller average coordination number. Indeed, it was previously observed that an increase in Poisson's ratio is strongly correlated with a decrease in average coordination number, which was specifically outlined for various borate glasses as well as for other glass families.[60], [61], [62] Hence, it is inferred that these structural reorganizations ultimately give rise to an increase in Poisson's ratio.

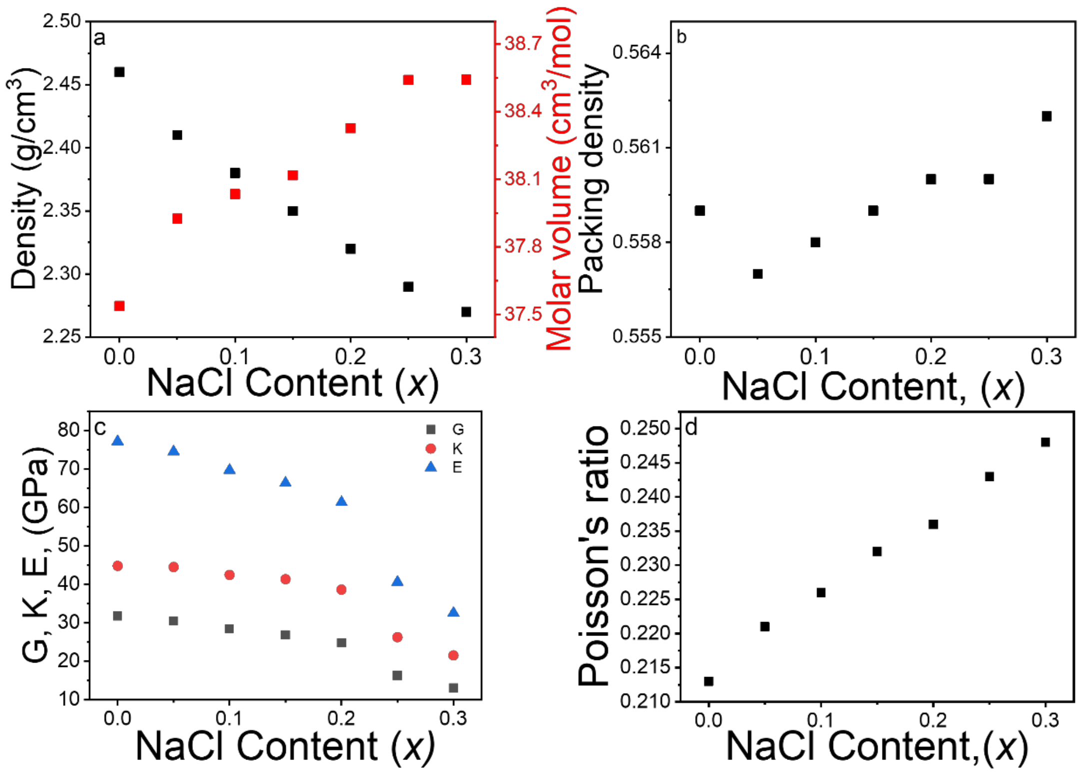

Figure 11. *Compositional dependence of* $[(Na_2O)_{0.4-x/2}(NaCl)_x](B_2O_3)_{0.48}(P_2O_5)_{0.12}$ *glasses on (a) density and molar volume, (b) packing density, (c) shear modulus (G), bulk modulus (K), and elastic modulus (E), and (d) Poisson's ratio (v).*

4. Conclusion

Mixed-anion (O^{2-} and Cl^-) oxychloride glasses from the $NaCl$-Na_2O-B_2O_3-P_2O_5 chemical system were produced and characterized. Oxygen-to-chlorine substitution rates of around 4 % were experimentally achieved without noticeable crystallization of NaCl.

The combined Raman, FTIR, and 1D ^{31}P MAS-NMR spectroscopic analyses provided insights into the local structure and compositional dependence of PO_4 and BO_x polyhedra, providing insight on the local environment of Cl^- ions. As chlorine substitutes for oxygen, it preferentially forms Na^+ and Cl^- enriched regions within the glass network. As a consequence, the polymerization degree of backbone borophosphate network increases through the formation of P-O-B and P-O-P linkages, while the BO_4 to BO_3 ratio decreases in a disproportionation reaction. At large chlorine concentrations, NaCl crystallizes from the enriched regions.

The proposed mechanism of chlorine introduction, specific to borophosphate networks, was considered in the light of the MRN model, which further allowed to describe the physico-mechanical properties of these glasses. The electrical conductivity first increases by one order of magnitude, thanks to the increased mobility of Na^+ ions, and slightly decreases with further addition of Cl^- ions, following from the increased crosslinking density of the glass network and segregated NaCl-rich regions, which impede the motion of charge carriers. The decrease in dimensionality of the glass structure, and the formation of a sodium-deficient borophosphate network containing large regions of aggregated Na^+ and Cl^- ions, resulted in a significant decrease in elastic moduli G, K, and E by approximately 60%, contrasting with a substantial increase in Poisson's ratio from 0.213 to 0.248.

Data availability statement

The data that support the findings of this study are available from the corresponding author upon reasonable request.

Underlying and related material

Table S1. *Fitting parameters: positions, widths and integrated area of Raman bands associated with different vibrational species present in the examined glasses.*

Species		**NaCl, *x***						
		0	0.05	0.1	0.15	0.2	0.25	0.3
Position, cm^{-1}	P-O-B[18]	630	630	630	630	631	631	631
	Metaborate[20]			673	673	673	674	674
	$1BO_3+2BO_4$[24, 20]	722	721	720	719	718	716	715
	$2BO_3+1BO_4$[24, 20]	763	763	764	765	765	765	766
	Boroxol rings[24, 8, 22]				799	799	800	800
	Pentaborate[21]						895	895
	BO_4[20]	947	947	947	948	948	948	948
	$Q^0_{1,BOx}$[18]	980	980	980	980	980	980	980
	$Q^1_{1,BOx}$	1015	1013	1012	1011	1009	1008	1006
	NBO in $Q^1_{1,BOx}$[23]						1069	1070
	Q^0_{2BOx}[18]	1098	1100	1102	1105	1106	1107	1108
Rel. Int, %	P-O-B	0.30	0.34	1.04	2.00	2.04	1.03	1.16
	Metaborate			0.59	0.30	0.56	0.26	0.17
	$1BO_3+2BO_4$	16.08	16.11	17.76	17.41	16.17	7.83	7.77
	$2BO_3+1BO_4$	14.01	15.61	17.76	19.66	19.46	15.95	15.07
	Boroxol rings				1.16	1.42	1.29	1.65
	Pentaborate						6.62	7.77
	BO_4	18.5	16,6	13.6	14.27	11.60	13.54	12.61
	$Q^0_{1,BOx}$	30.33	28.92	17.76	12.34	15.45	9.19	5.92
	$Q^1_{1,BOx}$	5.93	5.22	12.27	11.74	11.25	18.02	22.65
	NBO in $Q^1_{1,BOx}$						10.59	10.78
	Q^0_{2BOx}	14.84	17.14	19.35	21.11	22.10	15.95	14.55

Table S2. *Fitting parameters positions, widths, and integral of all the peaks from different species of NMR measurements.*

Species		**NaCl, *x***						
		0	0.05	0.1	0.15	0.2	0.25	0.3
Position, ppm	Q^0_0	15.3	14.1					
	$Q^0_{1,BOx}$	5.1	4.9	5.1	3.2	4.5	2.0	3.3
	$Q^0_{1,BOx}$	1.7	1.5	1.5	0.1	0.7	-0.3	-0.1
	Q^0_{2BOx}	-3.3	-3.5	-4.4	-5.0	-4.9	-5.5	-5.5
	$Q^1_{1,BOx}$	-9.4	-10.0	-9.9	-9.9	-9.5	-9.9	-9.9
	$Q^0_{3,BOx}$			-11.0	-12.5	-12.5	-12.9	-12.3
Width, ppm	Q^0_0	6.0	7.0					
	$Q^1_{0,BOx}$	4.8	4.8	4.3	5.6	4.	5.4	4.4
	$Q^0_{1,BOx}$	4.6	4.2	5.9	4.5	4.9	4.0	4.4
	Q^0_{2Box}	9.4	9.8	8.0	7.7	8.1	7.5	7.1
	$Q^1_{1,BOx}$	14.3	10.8	7.5	6.9	9.0	8.1	7.9
	$Q^0_{3,BOx}$			17.0	12.0	12.	14.1	14.6
Rel. Int, %	Q^0_0	1.1	0.9					
	$Q^1_{0,BOx}$	33.6	26.7	9.8	9.5	3.2	2.3	0.8
	$Q^0_{1,BOx}$	14.4	10.4	23.0	6.6	7.8	1.8	2.5
	Q^0_{2BOx}	48.3	60.2	56.7	63.6	66.3	47.2	36.6
	$Q^1_{1,BOx}$	2.5	1.6	5.7	9.1	12.3	20.	19.0
	$Q^0_{3,BOx}$			4.6	10.9	10.1	28.3	40.9

Author contributions

PZ: Writing – Original Draft, Investigation. CC: Writing – Review & Editing, Validation, Investigation. JC: Writing – Review & Editing, Validation, Investigation. AD: Writing – Review & Editing, Validation, Investigation. LW: Writing – Review & Editing, Supervision, Conceptualization.

Competing interests

The authors declare that they have no competing interests.

Funding

This work has received funding from the European Research Council (ERC) under the European Union's Horizon 2020 research and innovation program (grant 681652), the German Research Foundation (grant CA2110/2) and the Carl Zeiss Foundation (Durchbrueche 2019).

Acknowledgement

The authors wish to thank their colleagues Yang Xia, Quyen Huyen Le, and Bruno Poletto Rodrigues for fruitful discussions related to the influence of structure on electrical conductivity. We further thank Nadja Mai (XRD and thermal analysis), Christian Zeidler (FTIR), Omar Benzine (Raman), and René Limbach (elastic properties) for valuable support in data acquisition.

References

[1] Calahoo, C.; Wondraczek, L., Ionic glasses: Structure, properties and classification. *Journal of Non-Crystalline Solids: X* 2020, *8*, 100054.https://doi.org/10.1016/j.nocx.2020.100054

[2] Onodera, Y.; Kohara, S.; Masai, H.; Koreeda, A.; Okamura, S.; Ohkubo, T., Formation of metallic cation-oxygen network for anomalous thermal expansion coefficients in binary phosphate glass. *Nature Communications* 2017, *8* (1), 15449.10.1038/ncomms15449

[3] Ujiie, S.; Inagaki, T.; Hayashi, A.; Tatsumisago, M., Conductivity of 70Li2S·30P2S5 glasses and glass–ceramics added with lithium halides. *Solid State Ionics* 2014, *263*, 57-61.https://doi.org/10.1016/j.ssi.2014.05.002

[4] Kato, A.; Yamamoto, M.; Sakuda, A.; Hayashi, A.; Tatsumisago, M., Mechanical Properties of Li2S–P2S5 Glasses with Lithium Halides and Application in All-Solid-State Batteries. *ACS Applied Energy Materials* 2018, *1* (3), 1002-1007.10.1021/acsaem.7b00140

[5] Wang, Y.; Osaka, A.; Miura, Y.; Takahashi, K., Effect of halide ions on Li+ ionic conductivity in oxyhalo-borate glasses. *Journal of Materials Research* 1987, *2* (5), 606-609.10.1557/JMR.1987.0606

[6] Nienhuis, E. T.; Saleh, M.; Marcial, J.; Kriegsman, K.; Lonergan, J.; Lipton, A. S.; Guo, X.; McCloy, J. S., Structural characterization of ZnSO4-K2SO4-NaCl glasses. *Journal of Non-Crystalline Solids* 2019, *524*, 119639.https://doi.org/10.1016/j.jnoncrysol.2019.119639

[7] Sandland, T. O.; Du, L.-S.; Stebbins, J. F.; Webster, J. D., Structure of Cl-containing silicate and aluminosilicate glasses: A 35Cl MAS-NMR study. *Geochimica et Cosmochimica Acta* 2004, *68* (24), 5059-5069: https://doi.org/10.1016/j.gca.2004.07.017

[8] Deb, B.; Ghosh, A., Correlation of macroscopic ion dynamics with microscopic length scale and modification of network structure in ion conducting mixed network former glasses. *Europhysics Letters* 2012, *97* (1), 16001.10.1209/0295-5075/97/16001

[9] Zielniok, D.; Cramer, C.; Eckert, H., Structure/Property Correlations in Ion-Conducting Mixed-Network Former Glasses: Solid-State NMR Studies of the System Na2O−B2O3−P2O5. *Chemistry of Materials* 2007, *19* (13), https://doi.org/10.1021/cm0628092

[10] Takebe, H.; Harada, T.; Kuwabara, M., Effect of B2O3 addition on the thermal properties and density of barium phosphate glasses. *Journal of Non-Crystalline Solids* 2006, *352* (6), 709-713.https://doi.org/10.1016/j.jnoncrysol.2005.11.066

[11] Ducel, J. F.; Videau, J. J., Physical and chemical characterizations of sodium borophosphate glasses. *Materials Letters* 1992, *13* (4), 271-274.https://doi.org/10.1016/0167-577X(92)90230-H

[12] Brauer, D. S.; Möncke, D., Introduction to the Structure of Silicate, Phosphate and Borate Glasses. In *Bioactive Glasses: Fundamentals, Technology and Applications*, Boccaccini, A. R.; Brauer, D. S.; Hupa, L., Eds. The Royal Society of Chemistry: 2016; https://doi.org/10.1039/9781782622017-00061

[13] Weber, M. J., Science and technology of laser glass. *Journal of Non-Crystalline Solids* 1990, *123* (1), 208-222.https://doi.org/10.1016/0022-3093(90)90786-L

[14] Şakar, E.; Alım, B.; Ertap, H.; Karabulut, M., An extensive survey on radiation protection features of novel hafnium iron-borophosphate glasses: Experimental and theoretical study. *Progress in Nuclear Energy* 2023, *160*, 104690.https://doi.org/10.1016/j.pnucene.2023.104690

[15] Braunger, M. L.; Escanhoela, C. A.; Fier, I.; Walmsley, L.; Ziemath, E. C., Electrical conductivity of silicate glasses with tetravalent cations substituting Si. *Journal of Non-Crystalline Solids* 2012, *358* (21), 2855-2861.https://doi.org/10.1016/j.jnoncrysol.2012.07.013

[16] Sellappan, P.; Rouxel, T.; Celarie, F.; Becker, E.; Houizot, P.; Conradt, R., Composition dependence of indentation deformation and indentation cracking in glass. *Acta Materialia* 2013, *61* (16), 5949-5965.https://doi.org/10.1016/j.actamat.2013.06.034

[17] Saranti, A.; Koutselas, I.; Karakassides, M. A., Bioactive glasses in the system CaO–

B2O3–P2O5: Preparation, structural study and in vitro evaluation. *Journal of Non-Crystalline Solids* 2006, *352* (5), 390-398.https://doi.org/10.1016/j.jnoncrysol.2006.01.042

[18] Christensen, R.; Olson, G.; Martin, S. W., Structural Studies of Mixed Glass Former 0.35Na2O + 0.65[xB2O3 + (1 – x)P2O5] Glasses by Raman and 11B and 31P Magic Angle Spinning Nuclear Magnetic Resonance Spectroscopies. *The Journal of Physical Chemistry B* 2013, *117* (7), 2169-2179.10.1021/jp308494a

[19] Yamashita, H.; Nagata, K.; Yoshino, H.; Ono, K.; Maekawa, T., Structural studies of 30Na2O–5SiO2–65[(1−x)P2O5–xB2O3] glasses by nuclear magnetic resonance, Raman and infrared spectroscopy. *Journal of Non-Crystalline Solids* 1999, *248* (2), 115-126.https://doi.org/10.1016/S0022-3093(99)00241-0

[20] Möncke, D.; Kamitsos, E. I.; Palles, D.; Limbach, R.; Winterstein-Beckmann, A.; Honma, T.; Yao, Z.; Rouxel, T.; Wondraczek, L., Transition and post-transition metal ions in borate glasses: Borate ligand speciation, cluster formation, and their effect on glass transition and mechanical properties. *The Journal of Chemical Physics* 2016, *145* (12), 124501.10.1063/1.4962323

[21] Gaylord, S.; Tincher, B.; Petit, L.; Richardson, K., Viscosity properties of sodium borophosphate glasses. *Materials Research Bulletin* 2009, *44* (5), 1031-1035.https://doi.org/10.1016/j.materresbull.2008.11.002

[22] Koudelka, L.; Mošner, P., Borophosphate glasses of the ZnO–B2O3–P2O5 system. *Materials Letters* 2000, *42* (3), 194-199.https://doi.org/10.1016/S0167-577X(99)00183-4

[23] Anastasopoulou, M.; Vasilopoulos, K. C.; Anagnostopoulos, D.; Koutselas, I.; Papayannis, D. K.; Karakassides, M. A., Structural and Theoretical Study of Strontium Borophosphate Glasses Using Raman Spectroscopy and ab Initio Molecular Orbital Method. *The Journal of Physical Chemistry B* 2017, *121* (17), 4610-4619.10.1021/acs.jpcb.7b01563

[24] Yano, T.; Kunimine, N.; Shibata, S.; Yamane, M., Structural investigation of sodium borate glasses and melts by Raman spectroscopy.: I. Quantitative evaluation of structural units. *Journal of Non-Crystalline Solids* 2003, *321* (3), 137-146.https://doi.org/10.1016/S0022-3093(03)00158-3

[25] Mantisi, B.; Adichtchev, S.; Sirotkin, S.; Rafaelly, L.; Wondraczek, L.; Behrens, H.; Marcenat, C.; Surovtsev, N. V.; Pillonnet, A.; Duval, E.; Champagnon, B.; Mermet, A., Non-Debye normalization of the glass vibrational density of states in mildly densified silicate glasses. *Journal of Physics: Condensed Matter* 2010, *22* (2), 025402.10.1088/0953-8984/22/2/025402

[26] Zargar, R.; Russo, J.; Schall, P.; Tanaka, H.; Bonn, D., Disorder and excess modes in hard-sphere colloidal systems. *Europhysics Letters* 2014, *108* (3), https://doi.org/10.1209/0295-5075/108/38002

[27] Pan, Z.; Benzine, O.; Sawamura, S.; Limbach, R.; Koike, A.; Bennett, T. D.; Wilde, G.; Schirmacher, W.; Wondraczek, L., Disorder classification of the vibrational spectra of modern glasses. *Physical Review B* 2021, *104* (13), https://doi.org/10.1103/physrevb.104.134106

[28] Duval, E.; Boukenter, A.; Achibat, T., Vibrational dynamics and the structure of glasses. *Journal of Physics: Condensed Matter* 1990, *2* (51), https://doi.org/10.1088/0953-8984/2/51/001

[29] Le, Q. H.; Palenta, T.; Benzine, O.; Griebenow, K.; Limbach, R.; Kamitsos, E. I.; Wondraczek, L., Formation, structure and properties of fluoro-sulfo-phosphate poly-anionic glasses. *Journal of Non-Crystalline Solids* 2017, *477*, 58-72.https://doi.org/10.1016/j.jnoncrysol.2017.09.043

[30] Gautam, C.; Yadav, A. K.; Singh, A. K., A Review on Infrared Spectroscopy of Borate Glasses with Effects of Different Additives. *International Scholarly Research Notices* 2012, *2012* (1), 428497.https://doi.org/10.5402/2012/428497

[31] Hudgens, J. J.; Martin, S. W., Glass Transition and Infrared Spectra of Low-Alkali, Anhydrous Lithium Phosphate Glasses. *Journal of the American Ceramic Society* 1993, *76* (7), 1691-1696.https://doi.org/10.1111/j.1151-2916.1993.tb06636.x

[32] Abdelghany, A. M.; ElBatal, F. H.; ElBatal, H. A.; EzzElDin, F. M., Optical and FTIR structural studies of CoO-doped sodium borate, sodium silicate and sodium phosphate

glasses and effects of gamma irradiation-a comparative study. *Journal of Molecular Structure* 2014, *1074*, 503-510.https://doi.org/10.1016/j.molstruc.2014.06.011

[33] Scholze, H., The Nature of Water in Glass, II. *Glastech. Ber.* 1959, *32* (4), 142-52

[34] Efimov, A. M.; Kostyreva, T. y. G.; Sycheva, G. A., Water-related IR absorption spectra for alkali zinc pyrophosphate glasses. *Journal of Non-Crystalline Solids* 1998, *238* (1), 124-142.https://doi.org/10.1016/S0022-3093(98)00579-1

[35] Petit, L.; Cardinal, T.; Videau, J. J.; Durand, E.; Canioni, L.; Martines, M.; Guyot, Y.; Boulon, G., Effect of niobium oxide introduction on erbium luminescence in borophosphate glasses. *Optical Materials* 2006, *28* (3), 172-180.https://doi.org/10.1016/j.optmat.2004.12.007

[36] Efimov, A. M.; Pogareva, V. G., Water-related IR absorption spectra for some phosphate and silicate glasses. *Journal of Non-Crystalline Solids* 2000, *275* (3), 189-198.https://doi.org/10.1016/S0022-3093(00)00250-7

[37] Takata, M.; Acocella, J.; Tomozawa, M.; Watson, E. B., Effect of Water Content on the Electrical Conductivity of Na2O≅3SiO2 Glass. *Journal of the American Ceramic Society* 1981, *64* (12), 719-724.https://doi.org/10.1111/j.1151-2916.1981.tb15894.x

[38] Balzer, R.; Behrens, H.; Reinsch, S.; Fechtelkord, M., Structural investigation of hydrous phosphate glasses. *Physics and Chemistry of Glasses - European Journal of Glass Science andTechnology Part B* 2019, *60* (2), 49-61.10.13036/17533562.60.2.041

[39] Stolper, E., Water in silicate glasses: An infrared spectroscopic study. *Contributions to Mineralogy and Petrology* 1982, *81* (1), 1-17.10.1007/BF00371154

[40] Ilievski, S., Dersch, O., Kinkel, S., Maldener, J., Zouine, A., Rauch, F., Haspel, R.; Krämer, F. W., Practical IR extinction coefficients for water in commercial glasses determined by nuclear reaction analysis". *Glastech. Ber* 2000, *73* (2), https://doi.org/10.34657/13131

[41] Raguenet, B.; Tricot, G.; Silly, G.; Ribes, M.; Pradel, A., Revisiting the 'mixed glass former effect'in ultra-fast quenched borophosphate glasses by advanced 1D/2D solid state NMR. *Journal of Materials Chemistry* 2011, *21* (44), 17693-17704. https://doi.org/10.1039/C1JM12350E

[42] Le, Q. H.; Calahoo, C.; Xia, Y.; Buchheim, J.; Bragatto, C. B.; Wondraczek, L., Optimization of electrical conductivity in the Na2O-P2O5-AlF3-SO3 glass system. *Journal of the American Ceramic Society* 2020, *103* (9), 4939-4956.https://doi.org/10.1111/jace.17150

[43] Chenu, S.; Werner-Zwanziger, U.; Calahoo, C.; Zwanziger, J. W., Structure and properties of NaPO3–ZnO–Nb2O5–Al2O3 glasses. *Journal of Non-Crystalline Solids* 2012, *358* (15), 1795-1805.https://doi.org/10.1016/j.jnoncrysol.2012.05.027

[44] Massiot, D.; Fayon, F.; Capron, M.; King, I.; Le Calvé, S.; Alonso, B.; Durand, J.-O.; Bujoli, B.; Gan, Z.; Hoatson, G., Modelling one- and two-dimensional solid-state NMR spectra. *Magnetic Resonance in Chemistry* 2002, *40* (1), 70-76.https://doi.org/10.1002/mrc.984

[45] Tricot, G.; Alpysbay, L.; Doumert, B. Solid State NMR: A Powerful Tool for the Characterization of Borophosphate Glasses *Molecules* [Online], 2020.10.3390/molecules25020428

[46] Ducel, J. F.; Videau, J. J.; Suh, K. S.; Senegas, J., Influence of calcium-hydroxyapatite on sodium borophosphate glasses 31P and 11B NMR investigations. *physica status solidi (a)* 1994, *144* (1), 23-30.https://doi.org/10.1002/pssa.2211440104

[47] Matecki, M.; Poulain, M. In *Cadmium and Lead Fluorohalide Glasses*, Materials Science Forum, Trans Tech Publ: 1988; pp 167-172. https://doi.org/10.4028/www.scientific.net/MSF.32-33.167

[48] El-Hofy, M.; Hager, I. Z., Ionic conductivity in lithium haloborate glasses. *physica status solidi (a)* 2003, *199* (3), 448-456.https://doi.org/10.1002/pssa.200306670

[49] Siwadamrongpong, S.; Koide, M.; Matusita, K., Prediction of chloride solubility in CaO–Al2O3–SiO2 glass systems. *Journal of Non-Crystalline Solids* 2004, *347* (1), 114-120.https://doi.org/10.1016/j.jnoncrysol.2004.07.063

[50] Christensen, R.; Olson, G.; Martin, S. W., Ionic Conductivity of Mixed Glass Former 0.35Na2O + 0.65[xB2O3 + (1 – x)P2O5] Glasses. *The Journal of Physical Chemistry B* 2013, *117* (51), 16577-16586.10.1021/jp409497z

[51] Malugani, J. P.; Robert, G., Conductivite ionique dans les verres LiPO3LiX (X = I, Br, Cl).

Materials Research Bulletin 1979, *14* (8), 1075-1081.https://doi.org/10.1016/0025-5408(79)90075-8

[52] Ingram, M. D., Ionic conductivity and glass structure. *Philosophical Magazine B* 1989, *60* (6), 729-740.10.1080/13642818908209739

[53] Minami, T.; Shimizu, T.; Tanaka, M., Structure and ionic conductivity of glasses in the ternary systems AgX(X = I, Br or Cl)Ag2OB2O3. *Solid State Ionics* 1983, *9-10*, 577-583.https://doi.org/10.1016/0167-2738(83)90298-9

[54] Nesbitt, H. W.; Henderson, G. S.; Bancroft, G. M.; Ho, R., Experimental evidence for Na coordination to bridging oxygen in Na-silicate glasses: Implications for spectroscopic studies and for the modified random network model. *Journal of Non-Crystalline Solids* 2015, *409*, 139-148.https://doi.org/10.1016/j.jnoncrysol.2014.11.024

[55] Greaves, G. N., EXAFS and the structure of glass. *Journal of Non-Crystalline Solids* 1985, *71* (1), 203-217.https://doi.org/10.1016/0022-3093(85)90289-3

[56] Shannon, R. D., Revised effective ionic radii and systematic studies of interatomic distances in halides and chalcogenides. *Foundations of Crystallography* 1976, *32* (5), 751-767 https://doi.org/10.1107/S0567739476001551

[57] Makishima, A.; Mackenzie, J. D., Direct calculation of Young's moidulus of glass. *Journal of Non-Crystalline Solids* 1973, *12* (1), 35-45.https://doi.org/10.1016/0022-3093(73)90053-7

[58] Allison, T., JANAF thermochemical tables. *NIST standard reference database* 1996, *13*, 1453

[59] Reed, J. J., Digitizing "The NBS Tables of Chemical Thermodynamic Properties: Selected Values for Inorganic and C1 and C2 Organic Substances in SI Units". *J Res Natl Inst Stand Technol* 2020, *125*, 125007.10.6028/jres.125.007

[60] Rouxel, T., Elastic Properties and Short-to Medium-Range Order in Glasses. *Journal of the American Ceramic Society* 2007, *90* (10), 3019-3039.https://doi.org/10.1111/j.1551-2916.2007.01945.x

[61] Gaafar, M. S.; Marzouk, S. Y.; Zayed, H. A.; Soliman, L. I.; Serag El-Deen, A. H., Structural studies and mechanical properties of some borate glasses doped with different alkali and cobalt oxides. *Current Applied Physics* 2013, *13* (1), 152-158.https://doi.org/10.1016/j.cap.2012.07.007

[62] Sidkey, M. A.; A., A. E.-M.; S., G. M.; S., A. E.-A. N.; L., A. E.-L.; and Youssof, I. M., Elastic and structural properties of vanadium–lithium–borate glasses. *Philosophical Magazine* 2008, *88* (11), 1705-1722.10.1080/14786430802279752